

ABSTRACT

Climate and Landscape Reconstruction of the Arroyo Chijuillita Member of the Nacimiento Formation, San Juan Basin, New Mexico: Providing Environmental Context to Early Paleocene Mammal Evolution

Adam J. Davis, M.S.

Mentor: Stacy Atchley Ph.D

Sedimentologic, stratigraphic, and paleopedologic attributes of an outcrop of the lower Paleocene Arroyo Chijuillita Member (Nacimiento Formation) in the Bisti/De-Na-Zin Wilderness Area (San Juan Basin, New Mexico) are studied to provide paleoenvironmental context for the Puercan North American Land Mammal Ages (NALMA). The outcrop intersects the middle and late Puercan (Pu2-Pu3) age and is ideal to assess potential causes of this turnover. Fluvial channel and laterally continuous sandstones and associated fine-grained floodplain deposits, including paleosols documenting variability in drainage and maturity, comprise the outcrop. Paleoclimatic reconstructions from paleosols indicate no change in climate, and evidence of regional tectonics effecting deposition is not observed. Spatial and temporal variability in paleopedologic and sedimentologic characteristics are interpreted to be the result of autocyclic channel avulsion/migration. These observations suggest that mammalian turnover (Pu2-Pu3) is likely the result of rapid evolution following the K-Pg boundary and/or competition from migration of mammalian species into the basin.

Climate and Landscape Reconstruction of the Arroyo Chijuillita Member of the Nacimiento
Formation, San Juan Basin, New Mexico:
Providing Environmental Context to Early Paleocene Mammal Evolution

by

Adam Davis, B.S.

A Thesis

Approved by the Department of Geosciences

Stacy Atchley, Ph.D., Chairperson

Submitted to the Graduate Faculty of
Baylor University in Partial Fulfillment of the
Requirements for the Degree
of
Master of Science

Approved by the Thesis Committee

Stacy Atchley, Ph.D., Chairperson

Daniel Peppe, Ph.D.

Joseph White, Ph.D.

Accepted by the Graduate School
May 2019

J. Larry Lyon, Ph.D., Dean

Copyright © 2019 by Adam J. Davis

All rights reserved

TABLE OF CONTENTS

LIST OF FIGURES	vi
LIST OF TABLES	vii
ACKNOWLEDGMENTS	viii
DEDICATION	ix
ATTRIBUTIONS	x
CHAPTER ONE	1
Climate and Landscape Reconstruction of the Arroyo Chijuillita Member of the Nacimiento Formation, San Juan Basin, New Mexico: Providing Environmental Context to Early Paleocene Mammal Evolution.....	1
<i>Introduction</i>	1
<i>Methods</i>	3
<i>Measured Sections</i>	3
<i>Paleosol Analysis</i>	3
<i>Geochemical Analysis</i>	7
<i>Mean Annual Precipitation Proxies</i>	7
<i>Mean Annual Temperature Proxies</i>	8
<i>Grainsize Analysis</i>	8
<i>Results</i>	9
<i>Depositional Facies</i>	9
<i>Paleosols</i>	10

<i>Paleoclimatic Reconstruction</i>	14
<i>Grainsize Analysis</i>	15
<i>Discussion</i>	19
<i>Paleoclimate</i>	19
<i>Landscape Evolution</i>	21
<i>Implications for Mammalian Turnover</i>	23
<i>Summary</i>	24
<i>Appendices</i>	26
<i>Appendix 1.A. Geochemical Data</i>	27
<i>Appendix 1.B. Descriptions of Pedotypes Observed at the Photopan Outcrop</i>	30
<i>Appendix 1.C. Paleoclimate Estimates from all Paleosols Observed at the Photopan Outcrop</i>	33
<i>Works Cited</i>	35

LIST OF FIGURES

Figure 1.1. Maps of San Juan Basin and Bisti/De-Na-Zin Wilderness Area and geochronologic constraint.....	4
Figure 1.2. Photopan Outcrop with Measured Section Transects.....	5
Figure 1.3. Stratigraphic and Paleopedologic Data from Measured Sections	11-12
Figure 1.4. Stratigraphic and Paleoclimatic Data from Measured Sections	13-14
Figure 1.5. Photographic Examples of Facies Identified at the Photopan Outcrop	15
Figure 1.6. Diagrammatic Profiles of Pedotypes from Photopan Outcrop.....	16
Figure 1.7. Common Pedologic/Stratigraphic Features Identified at the Photopan Outcrop	17
Figure 1.8. Gran Size Analysis Data Vs. Data from Measured Section 1	18
Figure 1.9. Geochemical and Paleobotanical Climate Estimates	20

LIST OF TABLES

Table 1.1. Observed Fluvial Facies and Architectural Elements.....	10
Table 1.2. Summary of Mean Annual Precipitation and Mean Annual Temperature Estimates.....	19

ACKNOWLEDGMENTS

This work was supported by the National Science Foundation (grants EAR-1325552 and EAR-1325544), the American Chemical Society Petroleum Research Fund (52822-DNI18), Bureau of Land Management National Landscape Conservation System grants, 2013 Southwest Section AAPG Scholarship, and 2013 ExxonMobil Global Geoscience Recruitment Grant. We thank Tom Williamson Steve Brusatte, Ross Secord, Utanah Denenclaw, Matt Heizler, and Brittany Abbuhl for assistance in the field. We would also like to thank Lee Nordt, and Steve Dworkin for their helpful comments.

DEDICATION

To my father James Davis, my mother Sherry Davis, my sisters Amber Brown and Heather O'Brien, and the many friends who have supported my efforts.

Most importantly this is dedicated to my wife Casie Davis and my daughter Margret MaryAnn. Without you I am nothing and with you I have everything.

ATTRIBUTIONS

Adam J. Davis is the primary author of this manuscript. He compiled the reference material, collected and compiled the data, wrote the body of the manuscript, and created the figures and Tables. Drs. Stacy Atchley, Daniel Peppe, and Thomas Williamson provided field guidance, advice, manuscript edits, and otherwise facilitated the production of the manuscript. Andrew G. Flynn provided field assistance and data from paleobotanical studies.

CHAPTER ONE

Climate and Landscape Reconstruction of the Arroyo Chijuillita Member of the Nacimiento Formation, San Juan Basin, New Mexico: Providing Environmental Context to Early Paleocene Mammal Evolution

This chapter is published as: Davis, A.J., Peppe, D.J., Atchley, S.C., Williamson, T.E., and Flynn, A.G., 2016. Climate and Landscape Reconstruction of the Arroyo Chijuillita Member of the Nacimiento Formation, San Juan Basin, New Mexico: Providing Environmental Context to Early Paleocene Mammal Evolution. *Palaeogeography, Palaeoclimatology, Palaeoecology*. V. 463. pp. 27-44.

Introduction

The San Juan Basin, located in northwestern New Mexico and southwestern Colorado, is a foreland basin that formed during the Laramide orogeny (Figure 1.1; Chapin and Cather, 1983). In the western portion of the San Juan Basin, a series of badlands of late Cretaceous through early Eocene sediments are exposed (Figures 1.1 and 1.2). The Paleocene Nacimiento Formation is bounded by unconformities and is typically underlain by the earliest Paleocene Ojo Alamo Sandstone and overlain by the early Eocene San Jose Formation. The Nacimiento Formation is divided into three members: the Arroyo Chijuillita, the Ojo Encino, and the Escavada Members (Williamson and Lucas, 1992; Figure 1.1C), which are readily recognized in the field by their lithologic and sedimentologic features (Williamson and Lucas, 1992; Williamson, 1996). In the northern portion of the San Juan Basin, the Arroyo Chijuillita, the focus of this study, overlies the trough cross-bedded Ojo Alamo Sandstone, and is characterized by drab mudstones, sandy mudstones to muddy sandstones, and sparse brightly colored (red and green) paleosols (Williamson and Lucas, 1992; Williamson, 1996). This is in contrast to

the Ojo Encino Mbr, which is identified by repetitive black-red-green-white banding representing bentonitic mudstones (black), variegated paleosols (red and green), and trough cross-bedded sandstones (white) (Williamson and Lucas, 1992; Williamson, 1996). The Escavada Mbr is identified by a predominance of sandstones and increased proportion of silcretes and is unconformably overlain by the Eocene San Jose Formation (Williamson and Lucas, 1992; Williamson, 1996). Paleomagnetic studies indicate that the Nacimiento Formation may span as much as ~7 myr during the early and middle Paleocene with the middle and late Puercan (Pu2-Pu3) constrained to C29n (Figure 1.1C) (Lindsay et al., 1978; 1981; Taylor and Butler, 1980; Butler and Lindsay, 1985; Williamson, 1996).

The Nacimiento Formation has long been studied for its diverse mammalian fossil faunas and contains the type faunas for the Puercan (Pu) and Torrejonian (To) North American Land Mammal Ages (NALMA) (e.g., Cope, 1882a, b, c; Marsh, 1889a, b; Marsh, 1894; Wood, H.E. et al., 1941; Archibald et al., 1987; Williamson, 1996; Lofgren et al., 2004). The middle and late Puercan NALMAs in the San Juan Basin are characterized by major, and apparently abrupt, species turnover between Pu2 and Pu3 (Williamson, 1996; Lofgren et al., 2004); however, the driver(s) of the Pu2-Pu3 mammalian turnover is uncertain.

In this study we focus on a 500 m laterally continuous outcrop exposure of a ~25 m thick section through the lower portion of the Arroyo Chijuillita Member in the Bisti/De-Na-Zin Wilderness Area in northwestern New Mexico that spans the Pu2-Pu3 transition (Figures 1.1 and 1.2). At the study location, referred to as the Photopan Outcrop, we reconstruct the spatial and temporal variability of paleosols and fluvial

facies through the Pu2-Pu3 transition to assess the influence of extrinsic (i.e., climatic, tectonic) and/or intrinsic (i.e., autocyclic channel migration) controls on depositional environments. We then examine the potential impacts these controls may have had on driving faunal turnover between Pu2 and Pu3.

Methods

Measured Sections

Six measured section transects along the relatively continuous exposures across the Photopan Outcrop are shown in Figure 1.2. Measured Sections 2, 3, 4 and 6 intersect five conspicuous channel sandstones, whereas Measured Sections 1 and 5 constrain the sedimentologic and stratigraphic variability across equivalent interchannel areas. Data collected through each section include grain size trends, paleosol distribution and characteristics (i.e., redoximorphic features and slickensides), fluvial aggradational cycle (FAC) boundaries (*sensu* Atchley et al., 2004), and the distribution of sedimentary and biological structures. Classification within fluvial architectural elements and associated facies is after the scheme of Miall (1978; 1985). Outcrop sedimentologic, stratigraphic, and paleopedologic relationships are traced laterally to constrain the stratigraphic framework.

Paleosol Analysis

Paleosols are categorized into seven pedotypes based on similar attributes and master and subordinate horizon designations (*sensu* Retallack, 1994; Soil Survey Staff, 1999). Sampling and description of representative examples of each pedotype for texture, ped structure, color, iron redoximorphic features, and slickensides follow the guidelines of Soil Survey Staff (1999). Each paleosol, based on its pedotype designation, is assigned

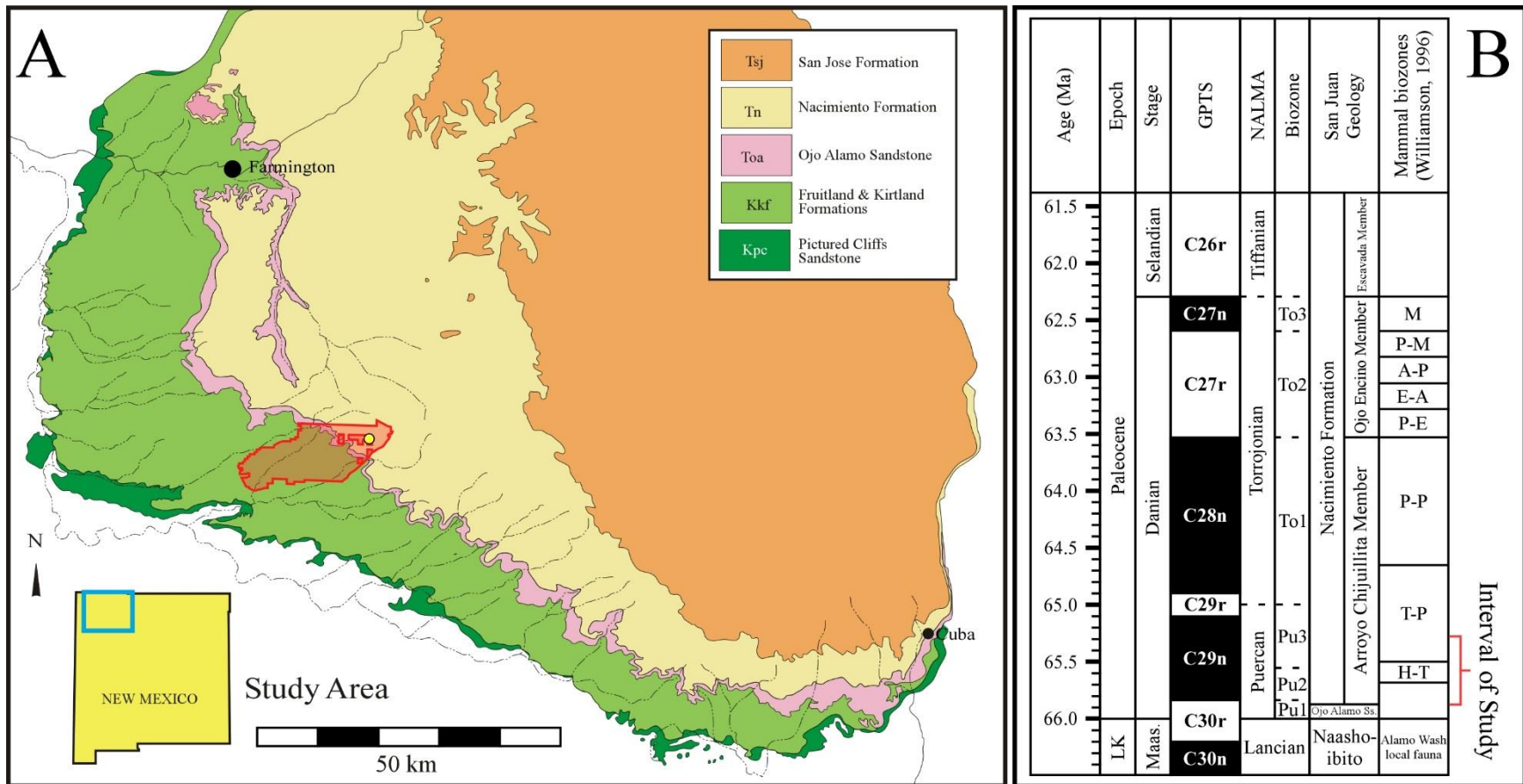


Figure 1.1: A) Geologic map of the San Juan Basin showing Cretaceous-Eocene sediments (modified from Williamson et al., 2008). Bisti/De-Na-Zin Wilderness Area is shown outlined in red and the Photopan Outcrop is designated by a yellow circle. B) Late Cretaceous and early Paleocene stratigraphy (Williamson, 1996) and chronologic constraint in the San Juan Basin (Butler and Lindsay, 1985; Ogg, 2012; Peppe et al., 2013, 2015). Geomagnetic Polar Time Scales (GPTS) after Ogg (2012). North American Land Mammal Ages (NALMA) from Lofgren et al. (2004). Mammal biozones specific to the San Juan basin after Williamson (1996). Interval of study is bracketed in red.

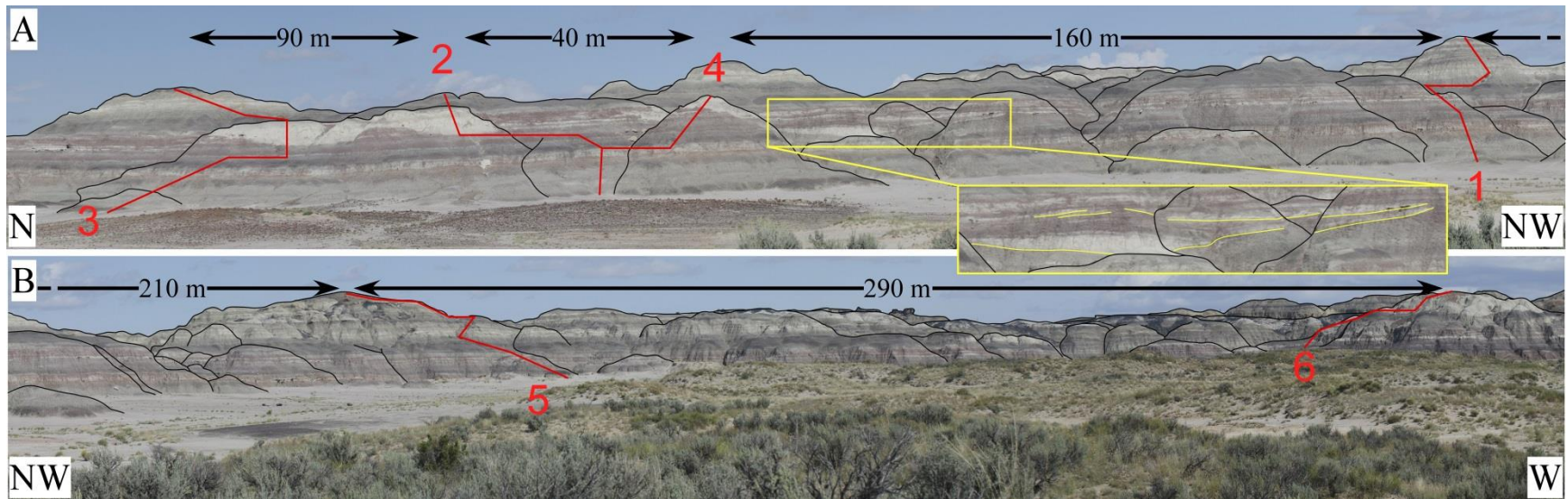


Figure 1.2: Photopanorama of Photopan Outcrop (Arroyo Chijuillita Member) from north (A) to west (B). Measured section transects are plotted in red. Expanded view of outcrop in yellow box shows scour surfaces (yellow lines) and associated lateral accretion deposits.

a maturity index (MI) based on composite B horizon thickness (Retallack, 1988; Trendell et al., 2012). Paleosol maturity is considered to be a qualitative indicator of landscape stability as increasing paleosol thickness and horizonation requires increased weathering time (Retallack, 1988). These index values range from 0 (0cm of B horizon) to 4 (over 150 cm of B horizon). Paleosol color and hydromorphic features are used to evaluate paleosol drainage. Although paleosol colors are commonly considered to be, at least somewhat, altered as a result of diagenetic changes to iron bearing minerals (Blodgett et al., 1993; Retallack, 2001), all paleosols in the study interval have been subjected to the same diagenetic conditions. PiPujol and Buurman (1994) discuss three possible origins of red colors in paleosols (a result of Fe (III) bearing minerals) which are: inherited color from parent material, early diagenesis, or late diagenesis. Inherited parent material coloration is not a reasonable explanation, as non-red C horizons are commonly observed below reddened B horizons in paleosols at the Photopan Outcrop. Also, following the arguments of PiPujol and Buurman (1994), late diagenesis is not preferred as this process would be expected to transform all iron bearing compounds similarly. However, the variety of red paleosol coloration across the outcrop, and within individual paleosols, indicates that late diagenetic conditions did not significantly alter the iron bearing minerals. As such, early diagenesis, or preserved soil coloration, is the best explanation of observed paleosol colors. Therefore, paleosol color is considered a qualitative proxy for original mineralogy resulting from differing drainage conditions. Drainage index (DI) values are determined as follows: paleosols with predominantly gleyed colors or grey chroma = 1 are considered poorly-drained (DI=1); paleosols that are predominantly gray with chroma ≤ 2 are considered moderately-drained (DI=2); and paleosols that are

predominantly red with chroma >2 are considered to be well-drained (DI=3). Paleosol maturity and drainage index values are plotted against thickness along their respective measured sections to correlate spatial and temporal trends.

Geochemical Analysis

Bulk geochemistry data are derived from ICP-MS and ICP-AES analysis performed on A and B horizons at a commercial lab (ALS Minerals, Reno, NV). The bulk geochemistry of the paleosols is used to reconstruct mean annual precipitation (MAP) and mean annual temperature (MAT). Bulk geochemical data are provided in Appendix A.

Mean annual precipitation proxies. MAP is estimated using the CIA-K (V) and CALMAG geochemical proxies from Nordt and Driese (2010). These relationships rely on the concept that base forming oxides (CaO, MgO, Na₂O, and K₂O) become depleted relative to Al₂O₃ with increased weathering driven by increased rainfall (Sheldon et al., 2002; Nordt and Driese, 2010; Adams et al., 2011; Atchley et al., 2013; Trendell et al., 2013; Beverly et al., 2015). CIA-K (V) and CALMAG use oxide mole percent and are calibrated to modern Vertisol B-horizons and are, therefore, applied only to paleosols interpreted to represent this soil order. CIA-K (V) is related to base forming cations using the equation $CIA-K (V) = [Al_2O_3 / (Al_2O_3 + CaO + Na_2O)] \times 100$ with the resultant index values related to MAP linearly as: $MAP (mm) = 18.64 (CIA-K (V)) - 350.4$ ($r^2 = 0.81$; $SE = \pm 146$ mm/yr). CALMAG is defined as $[Al_2O_3 / (Al_2O_3 + CaO + MgO)] \times 100$, with MAP estimated linearly as: $MAP (mm) = 22.69(CALMAG) - 435.8$ ($r^2 = 0.90$; $SE = 108$ mm/yr). As a result of their regressions, CALMAG always gives higher MAP estimates than CIA-K (V) (Nordt and Driese, 2010).

Mean annual temperature proxies. Mean annual temperature (MAT) is estimated using the salinization proxy of Sheldon et al. (2002) and the Paleosol Weathering Index of Gallagher and Sheldon (2013). The salinization proxy uses the relationship between temperature and the molecular ratio of Na₂O and K₂O to Al₂O₃ using the following equation $\text{MAT} = -18.516 ((\text{Na}_2\text{O} + \text{K}_2\text{O})/\text{Al}_2\text{O}_3) + 17.29$ ($r^2 = 0.37$; $\text{SE} = \pm 4.4$ °C). This proxy is designed to be applicable to most soil orders, and thus is applied to all of the soil orders represented in the Photopan Outcrop. The Paleosol Weathering Index is defined as $\text{PWI} = 100 \times [(4.2 \times \text{Na}_2\text{O}) + (1.66 \times \text{MgO}) + (5.54 \times \text{K}_2\text{O}) + (2.05 \times \text{CaO})]$ where the molar ratio of oxide-based elements are used in the calculations; MAT is then calculated as $\text{MAT} = -2.74 \times \ln(\text{PWI}) + 21.39$ ($r^2 = 0.57$; $\text{SE} = \pm 2.1$ °C). The PWI proxy is only applicable to paleo-Inceptisols, Alfisols, and Ultisols, and is only applied to paleo-Inceptisols at the Photopan Outcrop.

Grain Size Analysis

Quantitative grain size data are from 44 mechanically (shaker table and sonic probe) and chemically (Sodium hexametaphosphate) disaggregated samples, several from each FAC in Measured Section 1 (Figures 1.2 and 1.3), analyzed using a Malvern Instruments Mastersizer 2000 with a Hydro 2000MU attachment using the associated Mastersizer 2000 software. Measured Section 1 is used for quantitative grain size analysis because it has no channel sandstone truncating FACs, does not have covered section, and, therefore, has the most continuous sedimentary record.

Results

Depositional Facies

The interval of interest consists of interbedded mudstones, siltstones, and sandstones that include four depositional facies (*sensu* Miall 1978, 1985) identified on the basis of grain size (lithology), and mechanical and biological structures. Facies descriptions are given in Table 1.1 and distributions are provided in Figures 1.3 and 1.4 with representative photographs of facies shown in Figure 1.5. Silcretes are observed in the section, but the origin of these silica rich, highly indurated, thin sediments is not well understood (Rains, 1981; Williamson et al., 1992). Generally, given the large amount of volcanic activity across the Western Interior of North America during the Late Cretaceous and early Paleocene (*sensu* Dickenson et al., 1988), we interpret these deposits to be devitrified and variably reworked volcanic ashes.

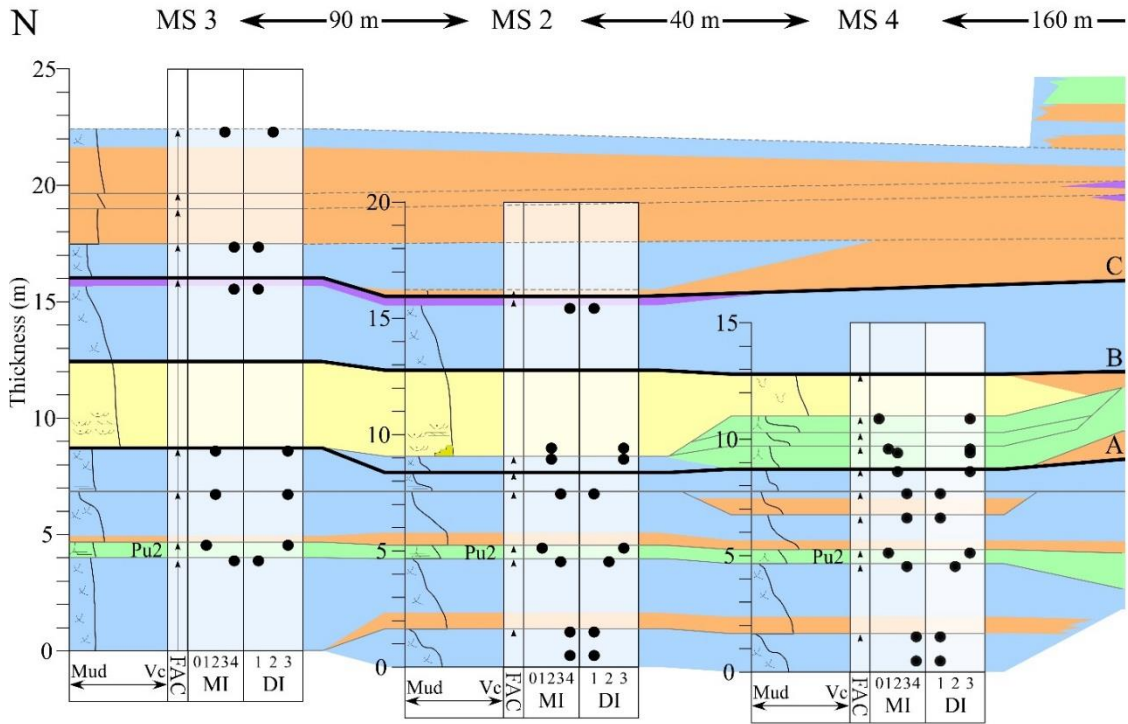
Pedogenically altered sediments are divided into proximal and distal floodplain on the basis of associated paleosol order. Paleo-Vertisols are considered to represent a relatively distal floodplain position (Fp) due to increased maturity and complete or near complete destruction of depositional bedforms via pedogenesis (Table 1.1 and Figure 1.5A). These features suggest relatively long periods of non-deposition and landscape stability. Paleo-Inceptisols and Entisols are considered to represent the proximal floodplain (Fh) because these paleosols have relatively little pedogenic alteration and abundant depositional bedforms (Table 1.1 and Figure 1.5B). Sand facies are found in two overall forms, lenticular shaped channel fills (Sl; Table 1.1 and Figure 1.5C) and laterally continuous proximal overbank deposits (Sm; Table 1.1 and Figure 1.5D).

Table 1.1: Fluvial facies and architectural elements (Miall, 1985) observed within the study interval.

Facies	Lithology	Description	Architectural Element
Fp	Mudstone	Unstratified clays to very fine sand; evidence of pedogenic alteration	Distal Floodplain (Vertisol)
Fh	Mudstone -Vf Sandstone	Laminated and horizontally bedded; clay-Vf sandstone; has minor to abundant drab root halos overprinting sedimentary structure	Proximal Floodplain (Inceptisol/Entisol)
Sl	Sandstone	Isolated, lenticular, fining upward fine to medium grained sandstone with scour base. Massive or with minor trough crossbedding and planar-tabular cross bedding	Lateral Accretion (point-bar channel fill from channel migration)
Sm	Sandstone	Relatively laterally continuous massive sandstones	Lateral Accretion/Proximal Overbank (non-pedogenically altered overbank)

Paleosols

Representative examples of pedotype profiles including maturity, drainage, and outcrop character are summarized in Figure 1.6, and detailed descriptions of pedotypes are provided in Appendix B. Subsurface horizons are restricted to Bss, Bssg, Bw, Bwg, C, and Cg horizons with no observed pedogenic and only minor diagenetic carbonate on ped surfaces. Gleyed designation to horizons is based on the presence of gleyed colors in the matrix or root halos (Appendix B). Macroscopic features are shown in hand samples in Figure 1.7. The most common features are ped structure, backfilled burrows (Figure 1.7A), slickensides (Figure 1.7B), and redoximorphic features including drab or oxidized root halos (Figures 1.7C, D, F, and G). Ped structure varies widely in regards to degree of development, size, and shape including large wedge peds and small angular platy peds. Slickensides (Figure 1.7B) are common and range from large-scale master surfaces to



Legend			
↑ FAC	∩ Burrows	∩ Rooting	∩ Trough Cross Bedding
	∩ Slickensides	— mm to cm Laminations	∩ Planar-Tabular Cross Bedding
Facies	Sand - lenticular (Sl)	Sand - massive (Sm)	
Silcrete	Floodplain fines - horizontally bedded (Fh)	Floodplain fines - unstratified (Fp)	

Figure 1.3: Stratigraphic and paleopedologic information from northern measured sections at Photopan Outcrop (Fig. 2). Western measured sections are shown in Fig. 3, con't below. Stratigraphic framework is constructed by correlating fluvial aggradational cycles (FAC) between measured sections (grey lines). A conspicuous red and green laminated bed found in each measured section is used as the datum. Facies and associated architectural elements are determined by sediment character and structures following Miall (1978; 1985). Complete facies descriptions are provided in Table 1. Pedotype maturity (MI) is based on composite B horizon thickness and paleosol drainage (DI) and is related to paleosol color. Bold horizons labeled A-C are interpreted to be surfaces (FAC boundaries or correlative surface) showing distal-proximal shifts in channel position. These are also shown in Fig. 4 and are related to quantitative grain size data in Fig. 8. Second panel of Fig. 3 with measured sections 1, 5, and 6 follows the same layout and uses the same acronyms.

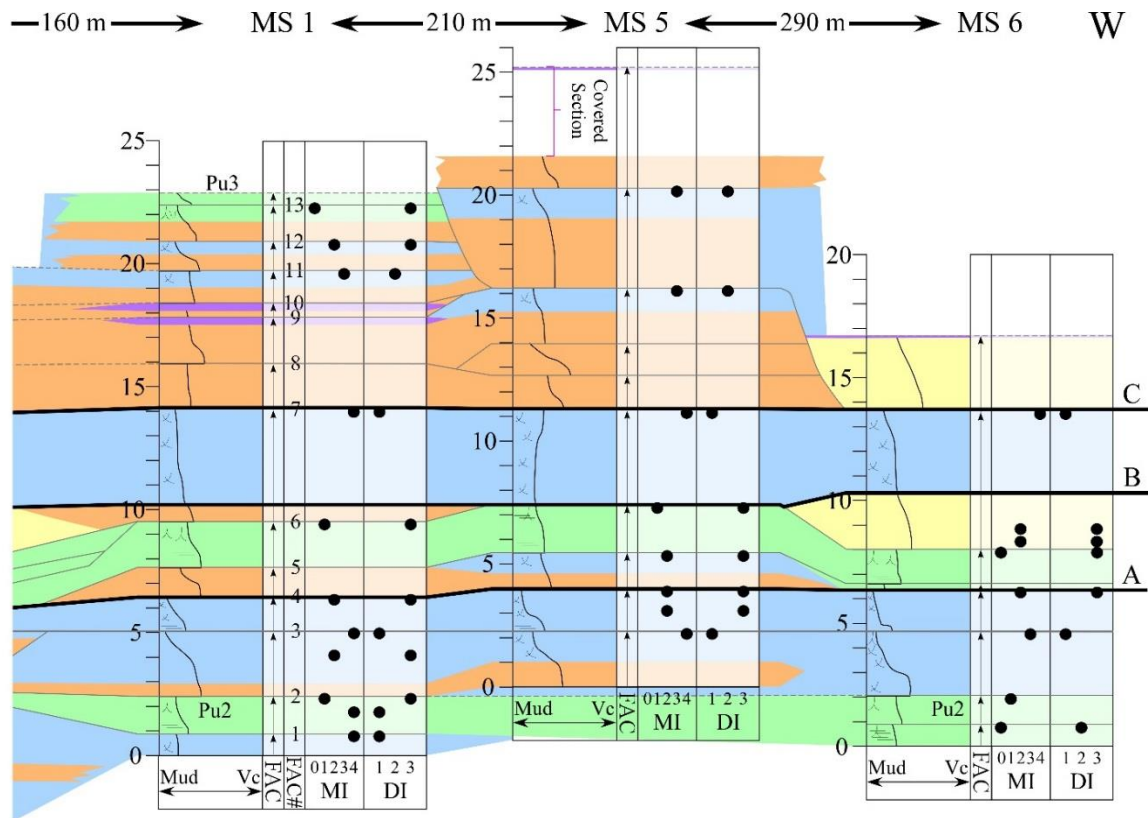
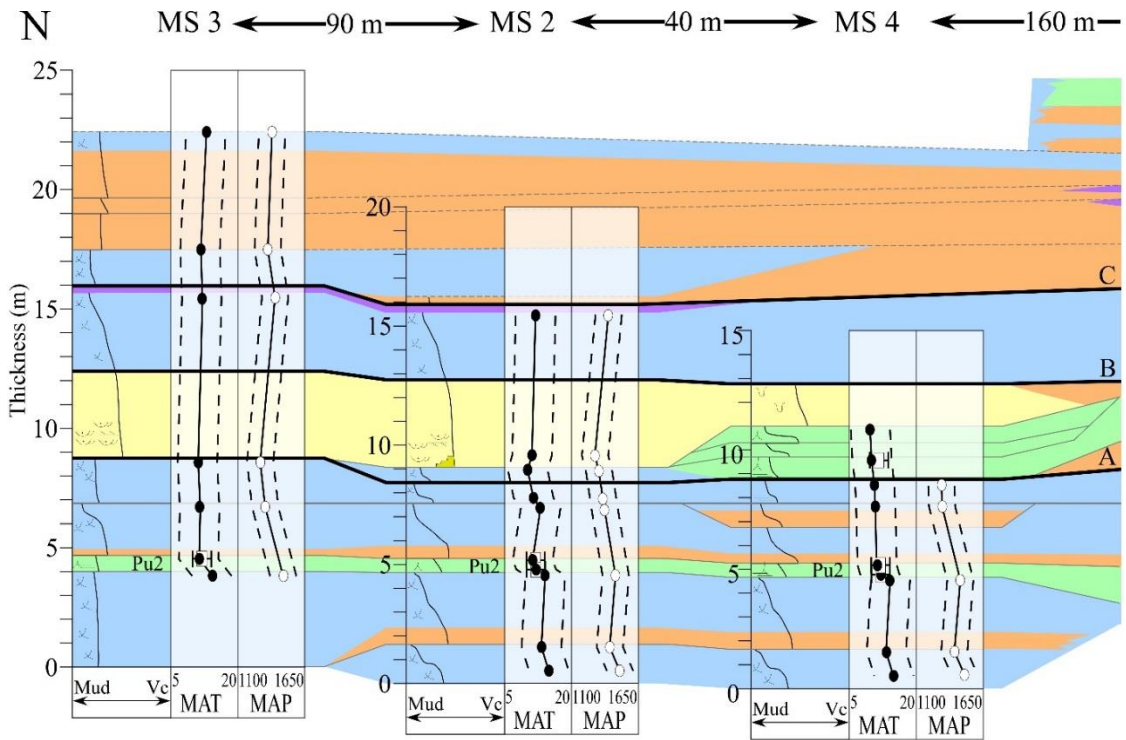


Figure 1.3 con't: Western portion of Photopan Outcrop (Fig. 2) showing stratigraphic and paleopedologic data continued from Fig. 3 above. Fluvial aggradational cycles (FAC) are numbered in measured section 1 for reference in discussion and in Fig. 8 below.

minor and/or incipient surfaces. Root traces are observed in two dominant forms: fine (mm to sub-mm thick), mat-like roots creating a “brecciated” appearance (Figure 1.7G), and thicker (cm) less densely rooted areas with downward bifurcation (Figure 1.7C and D). Additional redoximorphic features include Fe-nodules and areas of Fe-depletion and/or concentration (Figure 1.7C, G, and F). Burrows are most commonly drab clay or sand infilled in a drab matrix (Figure 1.7A). Figure 1.7E shows the bedding indicative of a C horizon with variegated overprinting. The paleosols in the Photopan Outcrop tend to have an inverse relationship between maturity and drainage (Figures 1.3 and 1.6).



Legend			Proxy Symbols
∩ Burrows	∩ Rooting	∩ Trough Cross Bedding	□ PWI with standard error
∩ Slickensides	∩ mm to cm Laminations	∩ Planar-Tabular Cross Bedding	○ CALMAG
Facies	Sand - lenticular (Sl)	Sand - massive (Sm)	● Salinization
Silcrete	Floodplain fines - horizontally bedded (Fh)	Floodplain fines - unstratified (Fp)	--- Margin of error for associated proxy

Figure 1.4: Mean annual temperature (MAT) and mean annual precipitation (MAP) estimates from geochemical proxies shown alongside stratigraphic and paleopedologic information and facies distributions from Fig. 3. CALMAG (Nordt and Driese, 2010) is applied only to paleo-Vertisols, PWI (Gallagher and Sheldon, 2013) is only applied to paleo-Inceptisols, and the salinization (Sheldon et al., 2002) is applied to all paleosols (paleo-Vertisols, Inceptisols, and Entisols). Ranges of paleosol geochemical proxy estimates are given in Table 2. As in Fig. 3, bold horizons labeled A-C are interpreted to be surfaces showing distal-proximal shifts in channel position. Second panel of Fig. 4 with measured sections 1, 5, and 6 follows the same layout and uses the same acronyms.

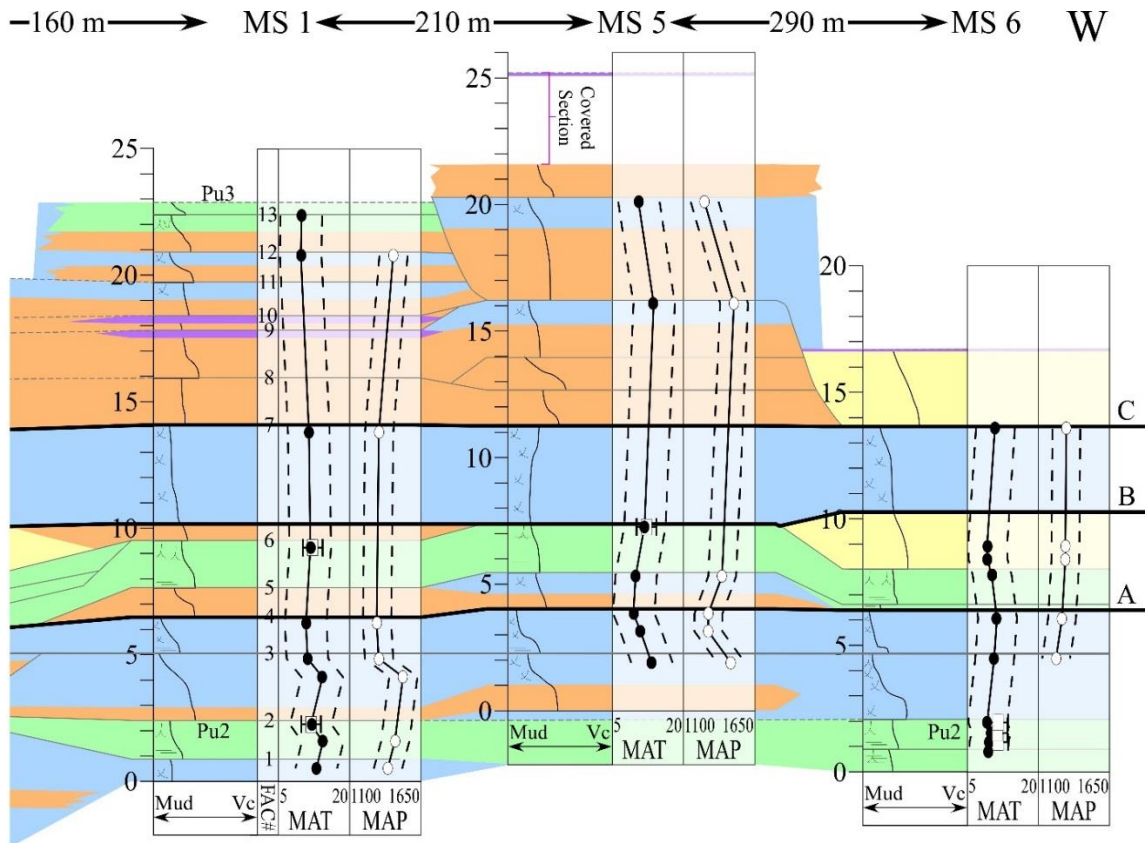


Figure 4 con't: Western portion of Photopan Outcrop (Fig. 2) showing MAT and MAP estimates continued from Fig. 4 above. As in Fig. 3 panel 2, fluvial aggradational cycles (FAC) are numbered in measured section 1 for reference in discussion and in Fig. 8 below.

Paleoclimatic Reconstruction

MAP estimates from CALMAG and CIA-K (V) give outcrop averages of 1372 (± 108) and 1150 (± 146) mm/yr, respectively, with no significant deviations observed throughout the study interval (Table 1.2, Figure 1.4, and Appendix C). All index values in the Photopan Outcrop are above 47.5; and therefore, all CALMAG MAP estimates are higher than estimates from CIA-K (V), which explains the differences in estimates between the proxies. MAT estimates from the salinization and PWI proxies give outcrop averages of 11.5 (± 4.4) and 12.0 (± 2.1) °C respectively, with no significant deviations observed (Table 1.2, Figure 1.4, and Appendix C). Figure 1.4 shows the CALMAG, salinization, and PWI estimates in stratigraphic context.

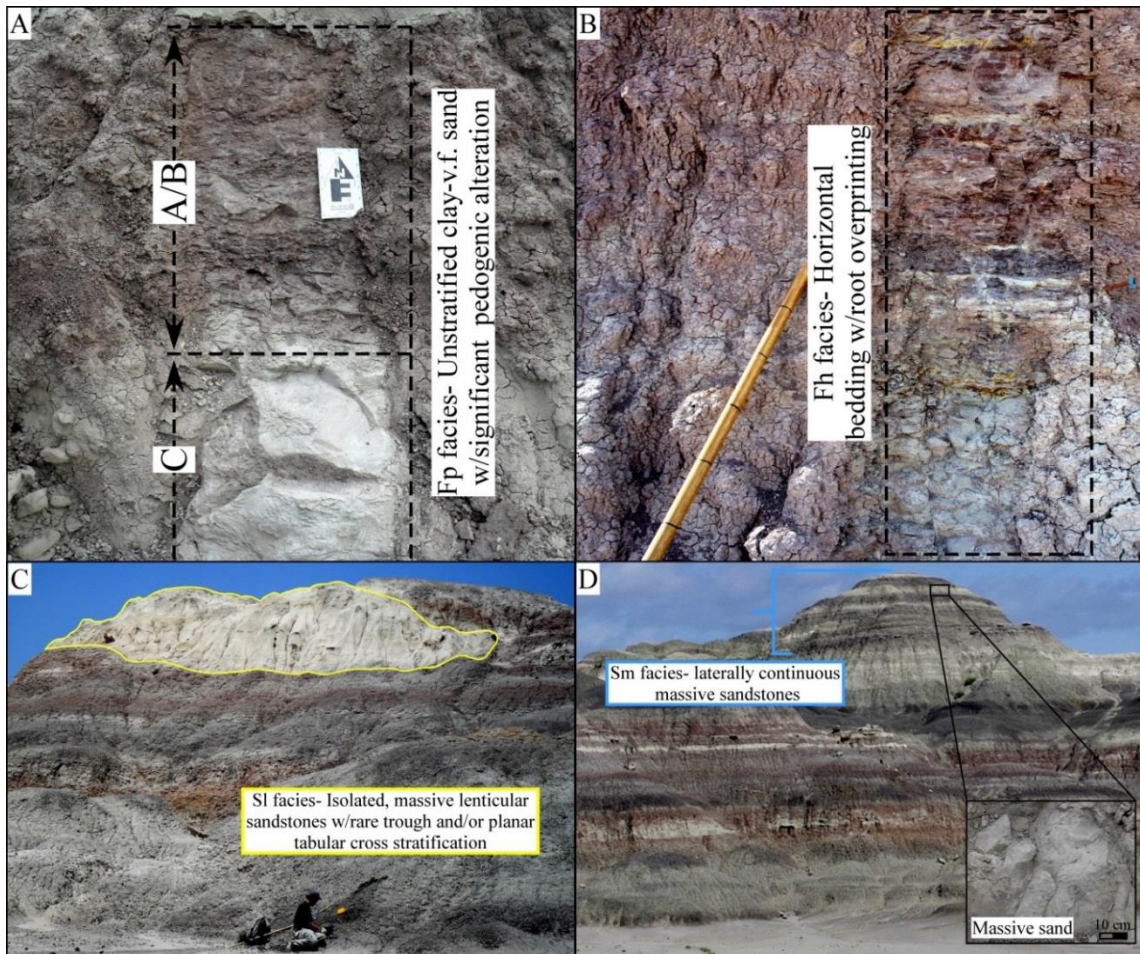


Figure 1.5: Outcrop examples of each facies from Table 1 and Figure 3. A) Pedotype 1 (Fp facies) from Measured Section 4. B) Fh facies in Measured Section 6. C) SI facies from Measured Sections 3 and 2. D) Laterally continuous Sm facies from top of measured section 3. Massive nature of sands is shown by inset image.

Grain Size Analysis

Sand/clay ratios from the quantitative grain size analysis of Measured Section 1 are shown in Figure 1.8 with facies distributions overlain. Measured Section 1 has an average sand/clay ratio of 0.37 with three significant positive excursions from the average that are coincident with Sm facies (Figure 1.8). Overall, higher sand/clay ratios align with facies interpreted to have been deposited proximal to the local channel

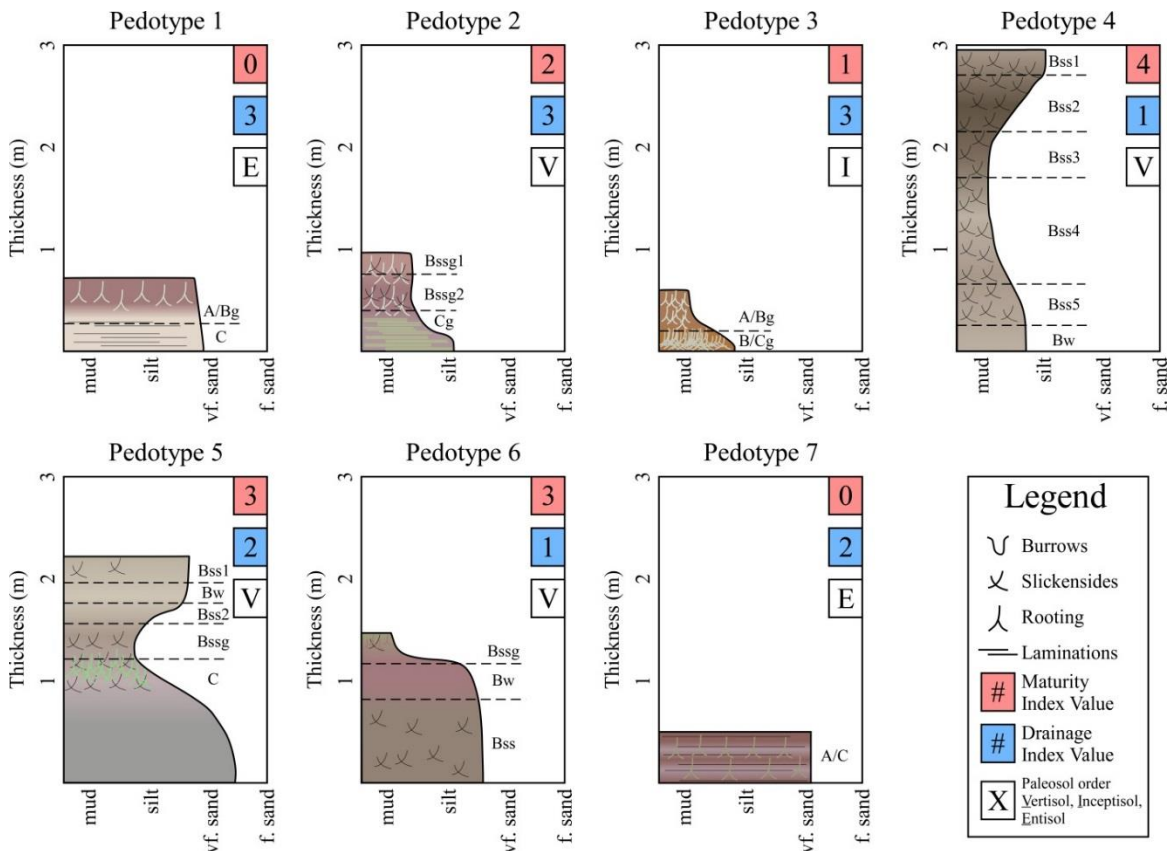


Figure 1.6: Diagrammatic profiles of pedotypes identified in Photopan Outcrop. Maturity index values 0-4 are based on composite thickness of B horizons (Retallack, 1988; Trendell et al., 2012) with higher values indicating more mature profiles. Drainage index values 1-3 are based on paleosol color with more red and higher chroma colors indicating increased drainage (Retallack, 2001). Horizon designations are given to the right of each profile. Detailed pedotype descriptions are provided in Appendix B.

(Sm, Sl, and Fh) and lower sand/clay ratios tend to align with facies (Fp) interpreted to be deposited distal to the local channel. This indicates an agreement between the facies interpretation and the quantitative grain size analysis, as proximal facies would be expected to be coarser grained (Figure 1.8).

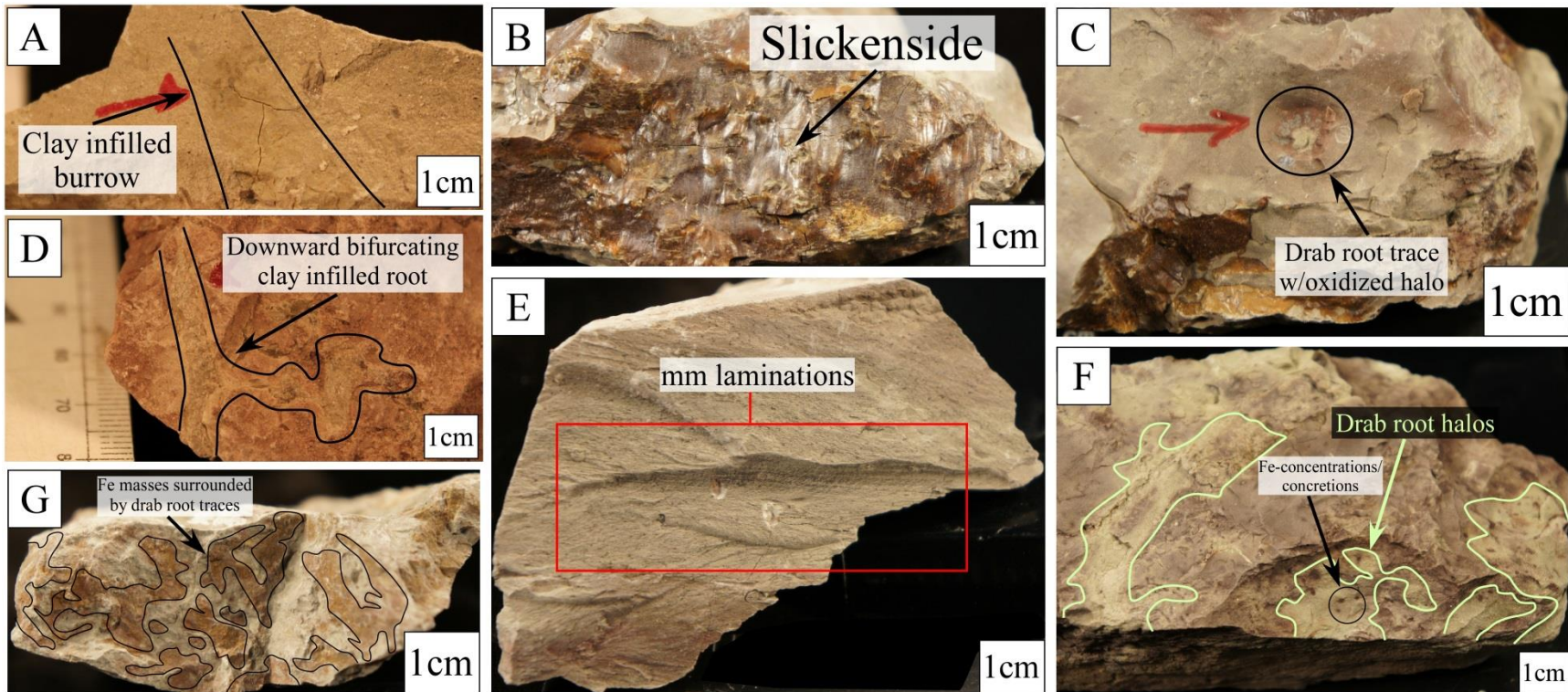


Figure 1.7: Photographs of paleosol hand samples showing prominent pedologic features. A) Clay infilled burrow from pedotype outlined in black. B) Well-developed slickensides from pedotype 2. C) Oxidized halo around drab root trace from pedotype 2. D) Downward bifurcating clay filled root trace from pedotype 1. E) Laminations in C horizon of pedotype 2. F) View of top of bedding plane from pedotype 7 showing variegated coloring including drab root traces (green outline) and purple Fe-concentrations (three outlined by black circle). G) Fine mat-like drab root traces and soft Fe-concretions/concentrations (outlined in black) from pedotype 3.

Measured Section 1

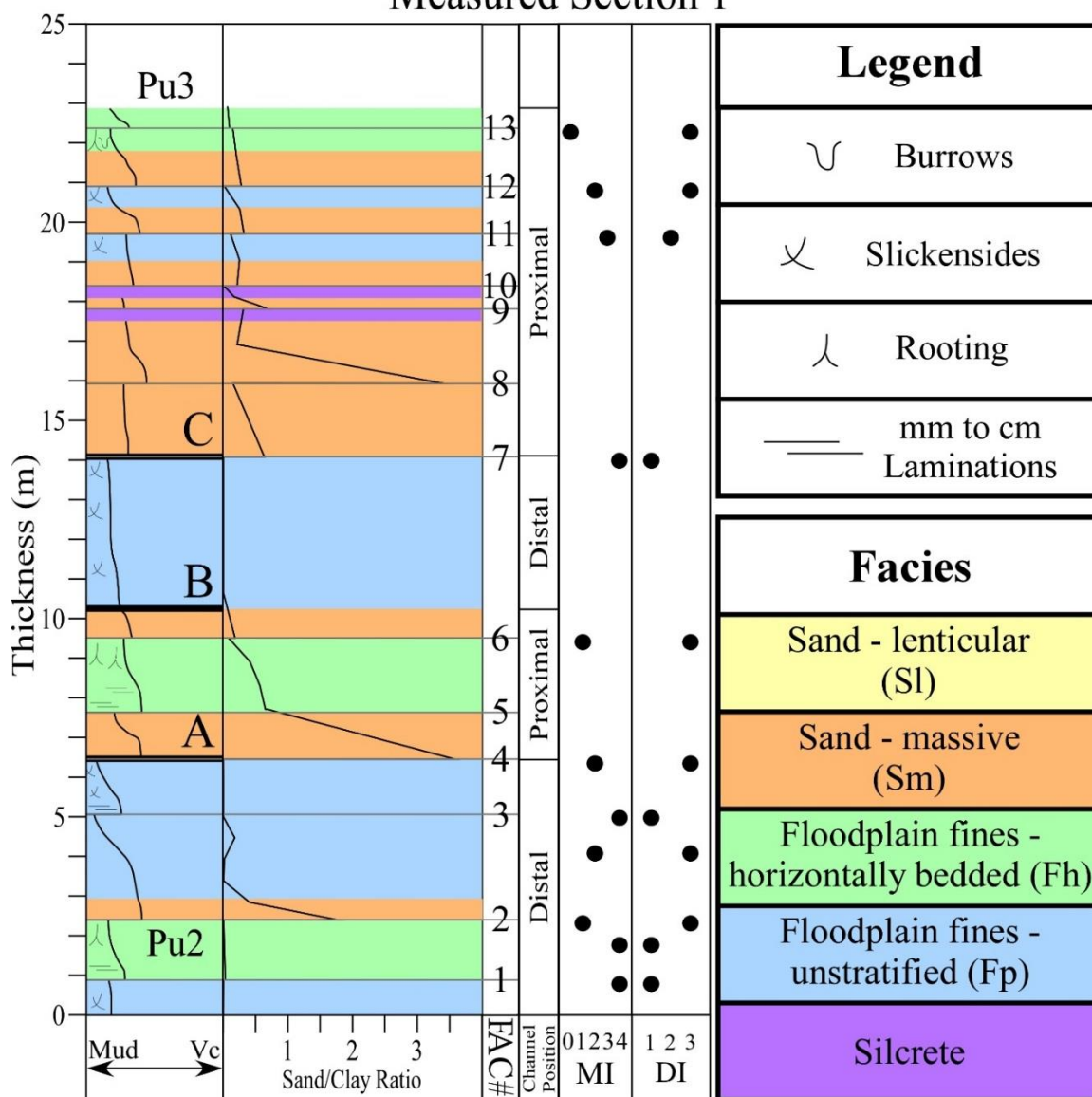


Figure 1.8: Sand/clay ratios from measured section 1 shown alongside stratigraphic data and paleosol indexes (maturity index- MI and drainage index- DI) from Figure 1.3 to interpret channel position. Shifts in distal-proximal channel position are also highlighted by bold lines labeled A, B, and C. These surfaces correspond across the landscape and are also shown in Figures 1.3 and 1.4. Fluvial aggradational cycles (FAC) numbering is from base to top and corresponds to numbering in first panel of Figures 1.3 and 1.4.

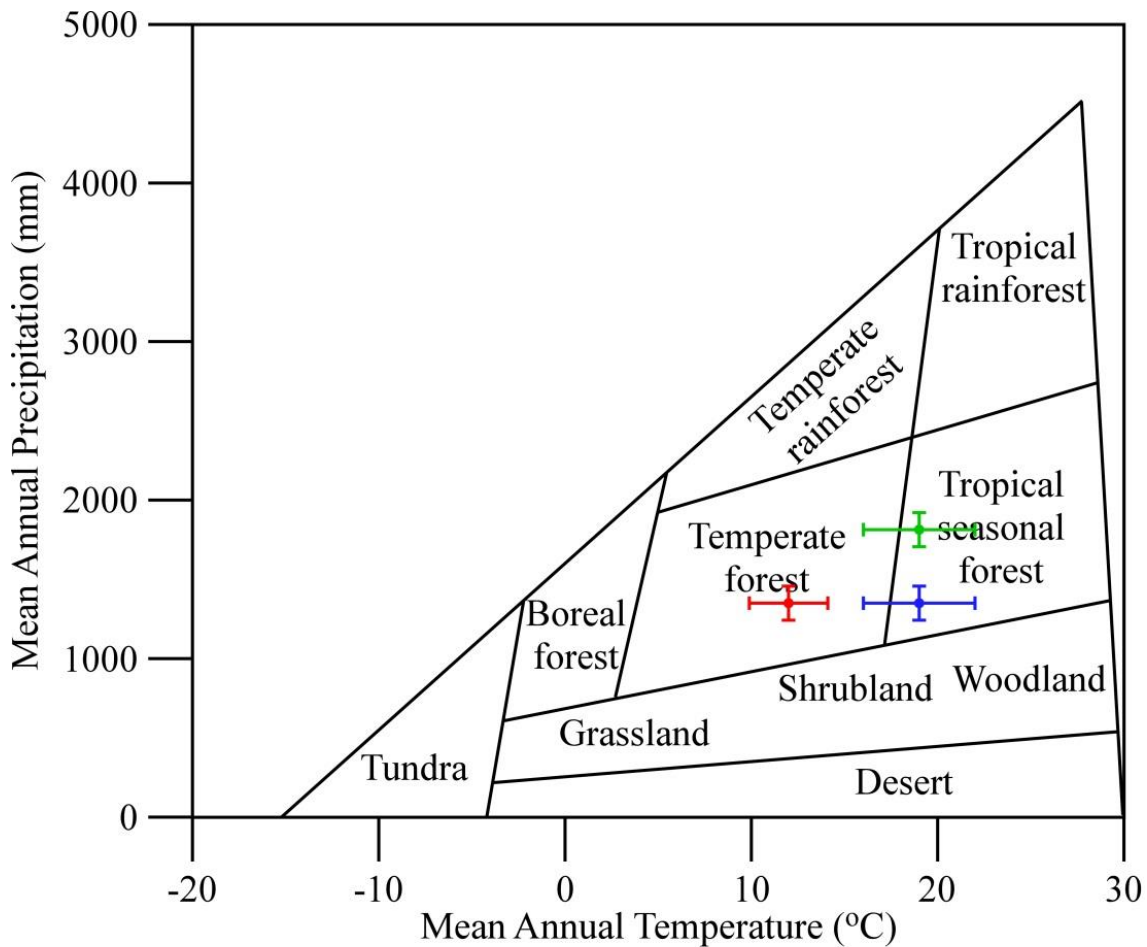
Table 1.2: Summary of MAP and MAT estimate ranges and averages from geochemically derived proxies.

Proxy [n]	Min	Max	Range	Average	Standard Error
CALMAG [33]	1241 mm/yr	1514 mm/yr	273 mm/yr	1372 mm/yr	± 108 mm/yr
CIA-K (V) [33]	1003 mm/yr	1342 mm/yr	339 mm/yr	1150 mm/yr	± 146 mm/yr
Salinization [47]	9.3 °C	15.1 °C	5.9 °C	11.5 °C	± 4.4 °C
PWI [10]	11.5 °C	12.3 °C	0.8 °C	12.0 °C	± 2.1 °C

Discussion

Paleoclimate

MAP estimates from CALMAG and CIA-K (V) are relatively consistent and neither proxy show temporal variability that would indicate a shift in MAP through the Pu2-Pu3 transition. Using Leaf Area Analysis (Wilf and Wing, 1998) on fossil leaves, Flynn et al. (2014) estimate a MAP of 1813 mm/yr (+1524/-828 mm/yr) for the Ojo Alamo Sandstone that underlies the Arroyo Chijuillita Mbr in the Bisti/De-Na-Zin Wilderness Area. Although the Ojo Alamo floras are slightly older than the sediments in the Photopan Outcrop and give significantly higher MAP than CIA-K (V), the paleobotanical MAP estimates are relatively consistent with the average CALMAG estimates (Table 1.2). Figure 1.9 shows this consistency as both CALMAG and Leaf Area Analysis MAP estimates plot in the temperate-tropical seasonal forest biomes of Whittaker (1975). Given the similarities between the CALMAG and paleobotanical MAP estimates, the commonality of Vertisols across the Photopan Outcrop, and a higher r^2 and lower standard error, we interpret CALMAG MAP estimates to be the most reasonable paleosol-derived values. Interestingly, the CALMAG and paleobotanical estimates suggest that MAP remained relatively constant from the deposition of the Ojo Alamo



MAP=CALMAG
MAT=LMA

MAP=CALMAG
MAT=PWI

MAP=LAA
MAT=LMA

Figure 1.9: Geochemical (this study) and paleobotanical (Flynn et al., 2014) climate estimates related to biomes after Whittaker (1975). LMA and LAA estimates are from the Ojo Alamo Sandstone and CALMAG estimates are from the overlying Arroyo Chijuillita Mbr of the Nacimiento Fm.

Sandstone through Pu3. Additionally, the preponderance of paleo-Vertisols in the Photopan Outcrop, identified mainly by the presence of shrink-swell features (slickensides), indicates seasonal drying of soil profiles.

MAT estimates from both salinization and PWI show no change through time and plot within the temperate forest biome of Whittaker (1975) (Figure 1.9). However, we consider a MAT of 11.5 – 12 °C to be a considerable underestimation, as these values are similar to high latitude, deep water ocean temperatures (e.g., Zachos et al., 2001) and the

same as or cooler than paleobotanical MAT estimates from contemporaneous deposits from North Dakota (Peppe, 2010; Peppe et al., 2011). Given the similarities between the paleosol MAT estimates from the San Juan Basin with those from considerably higher latitudes, we interpret the salinization and PWI estimates to be unreasonably low. Instead, we suggest that the paleobotanical MAT estimate of 19.0 °C (\pm 3.0 °C) using Leaf Margin Analysis (Wilf, 1997) from the underlying Ojo Alamo Sandstone (Flynn et al., 2014) is more reasonable. However, even though absolute MAT values derived from the paleosols are likely underestimates, we interpret the trend showing no evidence for significant changes in MAT to be reasonable.

Landscape Evolution

As discussed above, there is no evidence for climate change through the Pu2-Pu3 transition, and therefore, facies and paleosol variability at the Photopan Outcrop cannot be explained by changes in climate. Alternative drivers that could explain facies and pedotype distributions include regional tectonism or local autocyclic channel migration. Regional tectonism would require a complex relationship between tectonic pulsing and fluvial sedimentation to explain the spatial and temporal distributions of the sediments at the Photopan Outcrop. As such, if tectonism were a significant factor in sedimentation, autocyclic processes should not be able to fully account for facies shifts. However, our results indicate that autocyclic channel migration can account for the stratigraphic relationships seen at the Photopan Outcrop. Therefore, autocyclic channel migration provides a simpler and more plausible explanation for the spatial and temporal variability of facies and paleosols which are a function of channel proximity.

Eight to fourteen complete or partial fluvial aggradational cycles (FACs) are observed in measured sections across the Photopan Outcrop (Figures 1.3, 1.4, and 1.8). Several of these cycles are traceable across the outcrop; however, discontinuous cycles are also common. To simplify nomenclature, only FACs from Measured Section 1 are numbered (Figures 1.3, 1.4, and 1.8). Surfaces pertinent to landscape evolution interpretations are shown in bold and labeled A-C, and other spatial correlations of FACs are designated by grey lines (Figures 1.3, 1.4, and 1.8). Autocyclic channel migration toward and away from the Photopan Outcrop is interpreted from the recurring succession of observed facies, grain size, and paleosol character.

From the base of the section to FAC #4 sediments are relatively fine-grained and paleosols are mature and poorly-drained (Figures 1.3 and 1.8). The greater maturity of the paleosols and the fine-grained nature of the sediment indicate a distal channel position with less frequent sediment input. Above FAC #4 (surface A), sediments abruptly shift to coarser grained with relatively poorly-developed, but well-drained paleosols. The section from surface A to surface B, just above FAC #6, represents a proximal channel position. This is indicated by the association of S1 facies to the N and W of Measured Section 1 (Figures 1.2, 1.3, and 1.4). Additionally, the coarser grained sediment, scour surfaces, lateral accretion deposits, and the poorly-developed paleosols in this interval indicate regular sediment input causing interruption of pedogenesis (Figures 1.2 and 1.3). Above surface B there is an abrupt transition to fine grained Fp facies and associated mature and poorly-drained paleosols interpreted to be the result of channel avulsion and drift to a position distal to the Photopan Outcrop. The channel remains distal through FAC #7 (surface C). Above surface C the channel is interpreted to have drifted to a proximal

position, as is suggested by a return to coarser grained Sm and Sl facies (Figures 1.3, 1.4, and 1.8).

The landscape evolution described above is summarized in Figure 1.8 where distal/proximal channel positions are correlated to the cyclic succession of facies, sand/clay ratios, and paleosol maturity and drainage. Interestingly, positive excursions of sand/clay ratios generally coincide with surfaces (A-C) considered to represent channel avulsion events. This indicates agreement between the quantitative grain size analysis and the interpreted timing of avulsion events and landscape facies positions.

We interpret the relationship between trends of paleosol maturity and drainage to be related to channel proximity and landscape topographic position (Figures 1.3 and 1.6). Generally, paleosols further from a channel are both well-developed and well-drained; however, at the Photopan Outcrop, the best drained and most coarse grained paleosols developed proximal to the channel (Figures 1.3 and 1.6). We interpret these paleosols to have developed atop channel levees, i.e., topographically high and coarse grained due to channel proximity, and subsequently, better drained. The relatively continuous sediment input from flooding events, however, prevented levee-top paleosols from becoming well-developed. Landscape positions distal to channels are interpreted to be topographically lower and closer to the water table. Associated paleosols in these positions are poorly-drained, but due to limited sediment input, are also well-developed.

Implications for Mammalian Turnover

Throughout Pu2 and across the Pu2-Pu3 transition, there is no evidence for climatic variability and there is no evidence for tectonically driven changes in depositional environments. Therefore, neither climate nor regional tectonically driven

changes in depositional environments are plausible drivers for the Pu2-Pu3 transition. Autocyclic processes that affected the deposition in the Photopan Outcrop were ongoing throughout the entire Pu2-Pu3 interval and were also unlikely to have been regionally significant. Depositional autocyclicality, therefore, is unlikely to have influenced mammalian evolution and turnover. In the absence of changes in climate and regional changes in depositional environments, we suggest that the Pu2-Pu3 transition in the mammalian faunas was more likely driven by other intrinsic processes related to the mammalian communities, such as rapid evolution and speciation following the K-Pg boundary or competition related to migration of mammalian taxa into and out of the San Juan Basin (see Williamson, 1996; Lofgren et al., 2004).

Summary

There is no evidence of climatic change observed in the lower portion of the Arroyo Chijuillita Member at the Photopan Outcrop through the Pu2-Pu3 transition (Figure 1.4). MAP and MAT estimates from paleosols (this study) and from fossil leaves (Flynn et al., 2014) indicate that climate was warm and relatively wet (Figure 1.9). Additionally, vertic features in the paleosols throughout the section indicate seasonal precipitation. Therefore, changes in paleosol characteristics, specifically drainage and maturity, and the distribution of fluvial facies throughout the Photopan Outcrop are mostly likely the result of autocyclic channel migration and related landscape evolution.

Because climate is invariant and there is no evidence that regional tectonics influenced deposition, we suggest that turnover between Pu2 and Pu3 is most likely driven by intrinsic factors unrelated to environmental changes (e.g., rapid evolution

following the K-Pg boundary) or by competition from new mammalian species immigrating into the San Juan Basin.

APPENDICES

APPENDIX 1.A

Geochemical Data

Table A1: Geochemical data used in the calculation of estimates provided in Appendix C. All oxide % are calculated with standard conversion factors.

SAMPLE	Soil Order	Al	Al	Ca	Ca	K	K	Mg	Mg	Na	Na
DESCRIPTION	paleo-	oxide %	oxide mol ratio								
AD14_1_1	Vertisol	16.06	0.16	0.80	0.01	1.35	0.01	0.93	0.02	1.29	0.02
AD14_1_3	Vertisol	14.72	0.14	0.62	0.01	0.61	0.01	0.71	0.02	0.97	0.02
AD14_1_5	Inceptisol	17.35	0.17	0.49	0.01	2.51	0.03	0.85	0.02	1.36	0.02
AD14_1_7	Vertisol	17.46	0.17	0.64	0.01	0.78	0.01	0.66	0.02	1.23	0.02
AD14_1_8	Vertisol	15.68	0.15	0.77	0.01	2.17	0.02	1.21	0.03	1.66	0.03
AD14_1_10	Vertisol	14.62	0.14	0.76	0.01	1.95	0.02	1.16	0.03	1.71	0.03
AD14_1_11	Inceptisol	15.25	0.15	0.64	0.01	1.64	0.02	1.04	0.03	1.68	0.03
AD14_1_12	Vertisol	14.78	0.14	0.73	0.01	1.66	0.02	1.13	0.03	1.75	0.03
AD14_1_14	Vertisol	11.81	0.12	0.53	0.01	1.89	0.02	0.60	0.01	1.60	0.03
AD14_1_15	Entisol	14.36	0.14	0.77	0.01	2.22	0.02	1.28	0.03	1.97	0.03
AD14_2_1	Vertisol	14.85	0.15	0.73	0.01	1.75	0.02	0.99	0.02	1.60	0.03
AD14_2_3	Vertisol	13.98	0.14	0.63	0.01	0.94	0.01	0.56	0.01	1.29	0.02
AD14_2_6	Vertisol	14.78	0.14	0.84	0.01	2.16	0.02	1.04	0.03	1.97	0.03
AD14_2_8	Vertisol	15.49	0.15	0.77	0.01	1.99	0.02	1.31	0.03	1.75	0.03

AD14_2_9	Vertisol	15.46	0.15	0.74	0.01	1.31	0.01	0.86	0.02	1.77	0.03
AD14_2/4_1	Vertisol	19.37	0.19	0.77	0.01	0.31	0.00	0.75	0.02	1.19	0.02
AD14_2/4_3	Vertisol	17.19	0.17	0.81	0.01	1.34	0.01	0.91	0.02	1.28	0.02
AD14_2/4_7	Vertisol	17.44	0.17	0.69	0.01	0.80	0.01	0.81	0.02	1.20	0.02
AD14_2/4_9	Inceptisol	16.93	0.17	0.45	0.01	2.65	0.03	0.85	0.02	1.50	0.02
AD14_2/4_10	Inceptisol	17.50	0.17	0.52	0.01	2.47	0.03	0.90	0.02	1.29	0.02
AD14_3_1	Vertisol	15.91	0.16	0.57	0.01	0.64	0.01	0.71	0.02	1.02	0.02
AD14_3_2	Inceptisol	16.42	0.16	0.48	0.01	2.51	0.03	0.83	0.02	1.44	0.02
AD14_3_4	Vertisol	15.19	0.15	0.76	0.01	1.72	0.02	1.14	0.03	1.66	0.03
AD14_3_6	Vertisol	14.93	0.15	0.78	0.01	1.99	0.02	1.26	0.03	1.60	0.03
AD14_3_8	Vertisol	15.49	0.15	0.71	0.01	1.57	0.02	1.11	0.03	1.73	0.03
AD14_3_9	Vertisol	14.42	0.14	0.66	0.01	1.05	0.01	0.90	0.02	1.23	0.02
AD14_4_1	Vertisol	15.34	0.15	0.78	0.01	2.28	0.02	1.21	0.03	1.71	0.03
AD14_4_4	Vertisol	15.78	0.15	0.85	0.02	2.16	0.02	1.23	0.03	1.95	0.03
AD14_4_6	Inceptisol	14.17	0.14	0.66	0.01	2.37	0.03	1.18	0.03	1.77	0.03
AD14_4_8	Entisol	14.87	0.15	0.88	0.02	2.13	0.02	1.06	0.03	2.25	0.04
AD14_5_1	Vertisol	15.00	0.15	0.74	0.01	0.65	0.01	0.60	0.01	1.43	0.02
AD14_5_3	Vertisol	15.12	0.15	0.83	0.01	2.12	0.02	1.26	0.03	1.71	0.03
AD14_5_4	Vertisol	14.66	0.14	0.92	0.02	2.23	0.02	1.13	0.03	2.16	0.03
AD14_5_5	Vertisol	15.74	0.15	0.81	0.01	2.07	0.02	0.88	0.02	2.37	0.04
AD14_5_5.1	Inceptisol	14.51	0.14	0.73	0.01	1.51	0.02	1.26	0.03	1.58	0.03
AD14_5_6	Vertisol	15.81	0.16	0.60	0.01	0.58	0.01	0.66	0.02	1.44	0.02
AD14_5_7	Vertisol	14.51	0.14	0.70	0.01	2.07	0.02	1.41	0.03	1.75	0.03
AD14_6_1	Entisol	15.85	0.16	0.52	0.01	2.83	0.03	0.90	0.02	2.18	0.04
AD14_6_2.1	Inceptisol	15.42	0.15	0.52	0.01	2.72	0.03	0.85	0.02	2.04	0.03
AD14_6_2.6	Inceptisol	14.96	0.15	0.62	0.01	2.54	0.03	0.80	0.02	2.26	0.04

AD14_6_3	Vertisol	15.46	0.15	0.81	0.01	2.14	0.02	1.58	0.04	1.86	0.03
AD14_6_4.1	Vertisol	15.76	0.15	0.77	0.01	1.98	0.02	1.43	0.04	1.79	0.03
AD14_6_5	Entisol	14.53	0.14	0.77	0.01	2.29	0.02	1.31	0.03	1.78	0.03
AD14_6_6	Vertisol	14.40	0.14	0.87	0.02	2.20	0.02	1.08	0.03	2.28	0.04
AD14_6_7	Vertisol	15.51	0.15	1.04	0.02	2.13	0.02	1.08	0.03	2.41	0.04
AD14_6_8	Vertisol	15.51	0.15	0.85	0.02	1.82	0.02	1.18	0.03	2.01	0.03
AD14_6_2.3	Inceptisol	16.74	0.16	0.59	0.01	2.78	0.03	1.01	0.03	2.12	0.03

APPENDIX 1.B

Descriptions of Pedotypes Observed at the Photopan Outcrop

Table B1: Description of pedotypes found in Photopan Outcrop. Abbreviations M and D in Pedotype # column refer to pedotype maturity and drainage respectively.

Pedotype 1 (M=0; D=3)	Horizon	Depth (cm)	Colors	Structure*	Texture	Slicks †	Fe-features	Biologic	Sed-Structures
	A/Bg	0-45	7.5R 4/3 (75%; matrix); Gley1 8/10GY (25%; root halos)	1m	sandy siltstone	-	-	Clay infilled drab root halos	-
	C	45-70	5Y 8/1	0	sandy siltstone	-	-	-	Laminations
Pedotype 2 (M=2; D=3)	Horizon	Depth (cm)	Colors	Structure*	Texture	Slicks †	Fe-features	Biologic	Sed-Structures
	Bssg1	0-40	10R 4/3 (60%; matrix); Gley1 7/5GY (40%; root halos)	3mabk	silty mudstone	mp	-	-	-
	Bssg2	40-75	5R 4/3 (60%; matrix); Gley1 6/10Y (40%; root halos)	3m-cabk	mudstone	mp	-	-	-
	Cg	75-95	5R 5/2 (50%); Gley1 7/10Y (50%)	0	siltstone	-	-	-	Conspicuous red and green laminations (stratigraphic datum)

Pedotype 3 (M=1; D=3)	Horizon	Depth (cm)	Colors	Structure*	Texture	Slicks †	Fe-features	Biologic	Sed-Structures
	A/Bg	0-40	5YR 4/6 (60%; matrix); Gley1 7/5GY (40%; root halos)	1csbk	mudstone	-	Fe-oxide concentrations	Fine drab root halos	-
	B/Cg	40-60	Gley1 7/5GY (75%; matrix); 5YR 5/6 (25%; redoximorphic features)	1msabk	silty sandstone	-	Fe-oxide nodules	-	-
Pedotype 4 (M=4; D=1)	Horizon	Depth (cm)	Colors	Structure*	Texture	Slicks †	Fe-features	Biologic	Sed-Structures
	Bss1	0-25	2.5Y 5/1	3mabk	siltstone	ff	-	-	-
	Bss2	25-80	2.5Y 2.5/1	2m-csbk	silty mudstone	cd	-	-	-
	Bss3	80-125	2.5Y 3/1	3mabk	mudstone	cp	-	-	-
	Bss4	125- 230	2.5Y 6/1	2m-cabk	mudstone	cp	-	-	-
	Bss5	230- 270	2.5Y 5/1	3cwe	silty mudstone	cp	-	-	-
	Bw	270- 290	2.5Y 6/1	2cabk	silty mudstone	-	-	-	-
Pedotype 5 (M=3; D=2)	Horizon	Depth (cm)	Colors	Structure*	Texture	Slicks †	Fe-features	Biologic	Sed-Structures
	Bss1	0-25	5Y 6/2	1mabk-pl	sandy siltstone	ff	-	-	-
	Bw	25-45	5Y 7/2 (~3% 5R 4/2 oxidized root/burrows)	1cabk	sandy siltstone to vf sandstone	-	Oxidized root and/or burrows	-	-

	Bss2	45-65	2.5Y 5/1	2mabk	sandy mudstone	cp	-	-	-
	Bssg	65-100	5R 7/1 (50%); Gley1 7/10Y (50%)	2mbk	sandy mudstone	cd	-	Mottling of colors	-
	C	100-220		0	f-vf sandstone	-	-	-	Upward fining, sheet like
Pedotype 6 (M=3; D=1)	Horizon	Depth (cm)	Colors	Structure*	Texture	Slicks †	Fe-features	Biologic	Sed-Structures
	Bssg	0-30	Gley1 6/10Y (90%; matrix); 5R 4/4 (10%)	2cabk	mudstone	cd	Fe-oxide concentrations	-	-
	Bw	30-65	5YR 6/1	2c-vcsbk	sandy siltstone	-	-	-	-
	Bss	65-145	10YR 4/1	3m-cabk	sandy siltstone	cd	-	-	-
Pedotype 7 (M=0; D=2)	Horizon	Depth (cm)	Colors	Structure*	Texture	Slicks †	Fe-features	Biologic	Sed-Structures
	A/Cg	0-50	Verigated red (7.5R 3/4) to purple (5R 5/1) with drab root halo overprinting (Gley1 7/10Y to Gley1 7/5GY)	0	vf sandstone to sandy siltstone	-	Fe-oxide concentrations	Drab root halos increasing up profile	Thin bedding

* 0-structureless, 1-weak, 2-moderate, 3-strong grade; m-medium, c-coarse, vc-very coarse; sbk-subangular blocky, abk-angular blocky, we-wedge, pl-platy, m-massive type

† f-few, c-common, m-many abundance; f-faint, d-distinct, p-prominent

APPENDIX 1.C

Paleoclimate Estimates from all Paleosols Observed at the Photopan Outcrop

Table C1: All paleoclimate estimates from paleosols in Photopan Outcrop.

SAMPLE	Soil Order	MAP-CALMAG	CIA-K (V)	Salinization	PWI
DESCRIPTION	paleo-	MAP	MAP	MAT	MAT
AD14_1_1	Vertisol	1399	1174	13.2	-
AD14_1_3	Vertisol	1457	1223	14.4	-
AD14_1_5	Inceptisol	-	-	12.0	12.1
AD14_1_7	Vertisol	1515	1226	14.3	-
AD14_1_8	Vertisol	1331	1125	11.3	-
AD14_1_10	Vertisol	1317	1098	11.0	-
AD14_1_11	Inceptisol	-	-	11.8	12.3
AD14_1_12	Vertisol	1333	1101	11.4	-
AD14_1_14	Vertisol	1440	1078	9.9	-
AD14_1_15	Entisol	-	-	10.0	-
AD14_2_1	Vertisol	1367	1232	11.6	-
AD14_2_3	Vertisol	1481	1267	13.1	-
AD14_2_6	Vertisol	1334	1179	10.3	-
AD14_2_8	Vertisol	1304	1221	11.3	-
AD14_2_9	Vertisol	1411	1219	12.1	-
AD14_2/4_1	Vertisol	1504	1343	15.1	-
AD14_2/4_3	Vertisol	1424	1310	13.5	-
AD14_2/4_7	Vertisol	1472	1324	14.3	-
AD14_2/4_9	Inceptisol	-	-	11.5	12.0
AD14_2/4_10	Inceptisol	-	-	12.2	12.2
AD14_3_1	Vertisol	1489	1241	14.5	-
AD14_3_2	Inceptisol	-	-	11.6	12.1
AD14_3_4	Vertisol	1336	1117	11.7	-
AD14_3_6	Vertisol	1298	1115	11.3	-
AD14_3_8	Vertisol	1358	1121	11.9	-
AD14_3_9	Vertisol	1394	1174	13.2	-
AD14_4_1	Vertisol	1320	1110	10.9	-

AD14_4_4	Vertisol	1316	1081	10.8	-
AD14_4_6	Inceptisol	-	-	10.1	11.8
AD14_4_8	Entisol	-	-	9.8	-
AD14_5_1	Vertisol	1470	1145	13.5	-
AD14_5_3	Vertisol	1296	1099	11.0	-
AD14_5_4	Vertisol	1297	1024	9.8	-
AD14_5_5	Vertisol	1401	1039	10.1	-
AD14_5_5.1	Inceptisol	-	-	11.9	12.3
AD14_5_6	Vertisol	1495	1178	13.8	-
AD14_5_7	Vertisol	1266	1099	10.7	-
AD14_6_1	Entisol	-	-	9.5	-
AD14_6_2.1	Inceptisol	-	-	9.7	11.6
AD14_6_2.6	Inceptisol	-	-	9.3	11.6
AD14_6_3	Vertisol	1241	1091	10.8	-
AD14_6_4.1	Vertisol	1286	1110	11.3	-
AD14_6_5	Entisol	-	-	10.4	-
AD14_6_6	Vertisol	1311	1010	9.4	-
AD14_6_7	Vertisol	1313	1003	9.8	-
AD14_6_8	Vertisol	1320	1069	11.0	-
AD14_6_2.3	Inceptisol	-	-	10.1	11.5
Average		1373	1150	11.5	12.0

WORKS CITED

- Adams, J.S., Kraus, M.J., and Wing, S.L., 2011, Evaluating the use of weathering indices for determining mean annual precipitation in the ancient stratigraphic record: *Palaeogeography, Palaeoclimatology, Palaeoecology*, v. 309, p. 358-366, doi:10.1016/j.palaeo.2011.07.004.
- Archibald, J.D., Clemens, W.A., Gingrich, P.H., Krause, D.W., Lindsay, E.H., and Rose, K.E., 1987, First North American land mammal ages of the Cenozoic Era, *in* Woodbourne, M.O. ed, *Cenozoic mammals of North America*: Berkeley, University of California Press, p. 24-76.
- Atchley, S.C., Nordt, L., Dworkin, S, 2004, Eustatic control on alluvial sequence stratigraphy: a possible example from the Cretaceous-Tertiary transition of the Tornillo Basin, Big Bend National Park, West Texas, U.S.A: *Journal of Sedimentary Research*, v.74, p. 391-404, doi:10.1306/102203740391.
- Atchley, S.C., Nordt, L.C., Dworkin, S.I., Ramezani, J., Parker, W.G., Ash, S.R., and Bowring, S.A., 2013, A linkage among Pangean tectonism, cyclic alluviation, climate change, and biologic turnover in the Late Triassic: The record from the Chinle Formation, southwestern United States: *Journal of Sedimentary Research*, v.83, p. 1147-1161, doi: 10.2110/jsr.2013.89.
- Beverly, E.J., Driese, S.G., Peppe, D.J., Arellano, N., Blegen, N., Faith, J.T., Tryon, C.A., 2015, Reconstruction of a semi-arid late Pleistocene paleocatena from the Lake Victoria region, Kenya: *Quaternary Research*, v. 84, p. 368-381, doi:10.1016/j.yqres.2015.08.002.
- Blodgett, R.H., Crabaugh, J.P., and McBride, E.F., 1993, The color of red beds- a geologic perspective: *Soil Science Society of America*, v. 31, p. 127-159, doi:10.2136/sssaspecpub31.c8.
- Butler, R.F. and Lindsay, E.H., 1985, Mineralogy of magnetic minerals and revised magnetic polarity stratigraphy of continental sediments, San Juan Basin, New Mexico: *Journal of Geology*, v. 93, p. 535-554.

- Chapin, C.E. and Cather, S.M., 1983, Eocene tectonics and sedimentation in the Colorado Plateau- Rocky Mountain area: Arizona Geological Society Digest, v. 14, p. 173-198.
- Cope, E.D., 1882a, Synopsis of the vertebrata of the Puerco Eocene epoch: American Philosophical Proceedings, v. 20, p. 461-471.
- Cope, E.D., 1882b, A new genus of Taeniodonta: American Naturalist, v. 16, p. 604-605.
- Cope, E.D., 1882c, Some new forms from the Puerco Eocene: American Naturalist, v. 16, p. 833-834.
- Dickinson, W.R., Klute, M.A., Hayes, M.J., Janecke, S.U., Lundin, E.R., McKittrick, M.A., and Olivares, M.D., 1988, Paleogeographic and paleotectonic setting of Laramide sedimentary basins in the central Rocky Mountain region: Geological Society of America Bulletin, v. 100, p. 1023-1039, doi: 10.1130/0016-7606(1988)100<1023:PAPSOL>2.3.CO;2.
- Flynn, A., Peppe, D.J., Abbuhl, B., and Williamson, T., 2014, Early Paleocene floras from the San Juan Basin, New Mexico, USA: Implications for local and regional responses to the Cretaceous-Paleogene extinction event: Geological Society of America Abstracts with Programs, v. 46, no. 6, p. 757.
- Gallagher, T.M., and Sheldon, N.D., 2013, A new paleothermometer for forest paleosols and its implications for Cenozoic climate: Geology, v. 41, p. 647-650, doi:10.1130/G34074.1.
- Lindsay, E.H., Jacobs, L.L., and Butler, R.F., 1978, Biostratigraphy and magnetostratigraphy of Paleocene terrestrial deposits, San Juan Basin, New Mexico: Geology, v. 6, p. 425-429, doi: 10.1130/0091-7613(1978)6<425:BAMOPT>2.0.CO;2.
- Lindsay, E.H., Butler, R.F., and Johnson, N.M., 1981, Magnetic polarity zonation and biostratigraphy of Late Cretaceous and Paleocene continental deposits, San Juan Basin, New Mexico: American Journal of Science, v. 281, p. 390-435, doi: 10.2475/ajs.281.4.390.
- Lofgren, D.L., Lillegraven, J.A., Clemens, W.A., Gingrich, P.D., and Williamson, T.E., 2004, Paleocene biochronology: the Puercan through Clarkforkian land mammal ages, *in* Woodbourne, M.O., ed., Late Cretaceous and Cenozoic mammals of North America: New York, Columbia University Press, p. 43-105.
- Marsh, O.C., 1889a, Discovery of Cretaceous mammalia I, American Journal of Science, v. 38, p. 81-92.
- Marsh, O.C., 1889b, Discovery of Cretaceous mammalia II, American Journal of Science, v. 38, p. 177-180.

- Marsh, O.C., 1894, Description of Tertiary artiodactyls, *American Journal of Science*, v. 48, p. 259-274.
- Miall, A.D., 1978, Lithofacies types and vertical profile models of braided river deposits: A summary, *in* A.D. Miall, ed., *Fluvial sedimentology*: Canadian Society of Petroleum Geologists Memoir 5, p. 598-604.
- Miall, A.D., 1985, Architectural-element analysis: A new method of facies analysis applied to fluvial deposits: *Earth Science Reviews*, v. 21, p. 261-308.
- Nordt, L.C. and Driese, S.G., 2010, New weathering index improves paleorainfall estimates from Vertisols: *Geology*, v. 38, p. 407-410, doi: 10.1130/G30689.1.
- Ogg, J. G., 2012, Geomagnetic Polarity Time Scale, *in* Gradstein, F. M., Ogg, J. G., Schmitz, M. D., and Ogg, G. D., eds., *The Geologic Time Scale*: Oxford, UK, Elsevier, p. 85-114.
- Peppe, D.J., 2010, Megafloral change in the early and middle Paleocene in the Williston Basin, North Dakota, USA, *Palaeogeography, Palaeoclimatology, Palaeoecology*, v. 298, p. 224-234, doi:10.1016/j.palaeo.2010.09.027.
- Peppe, D.J., Royer, D.L., Cariglino, B., Oliver, S.Y., Newman, S., Leight, E., Enikolopov, G., Fernandez-Burgos, M., Herrera, F., Adams, J.M., Correa, E., Currano, E.D., Erickson, J.M., Hinojosa, L.F., Hoganson, J.W., Iglesias, A., Jaramillo, C.A., Johnson, K.R., Jordan, G., Kraft, N.J.B., Lovelock, E.C., Lusk, C.H., Niinemets, Ü., Peñuelas, J. Rapson, G., Wing, S.L., Wright, I.J., 2011, Sensitivity of leaf size and shape to climate: global patterns and paleoclimatic applications: *New Phytologist*, v. 190, p. 724-739, doi: 10.1111/j.1469-8137.2010.03615.x.
- Peppe, D.J., Heizler, M.T., Williamson, T.E., Masson, I.P., Brusatte, S., Weil, A., and Secord, R., 2013, New age constraints on the Late Cretaceous through Early Paleocene rocks in the San Juan Basin, New Mexico: *Geological Society of America Abstracts with Programs*, v. 45, no. 7, p. 290.
- PiPujol, M.D., and P. Buurman, 1994, The distinction between groundwater gley and surface-water gley phenomena in Tertiary paleosols of the Ebro Basin, northeast Spain: *Palaeogeography, Palaeoclimatology, Palaeoecology*, v. 110, p.103-113, doi:10.1016/0031-0182(94)90112-0.
- Rains, G.E., 1981, Paleocene silcrete beds in the San Juan Basin: unpublished M.S. thesis, Department of Geology, University of Arizona, 81pp.
- Retallack, G.J., 1988, Field recognition of paleosols, *in* J. Reinhardt and W.R. Sigleo, eds., *Paleosols and weathering through geologic time: Techniques and applications*: Geological Society of America Special Paper 216, p. 181-200, doi: 10.1130/SPE216-p1.

- Retallack, G.J., 1994, A pedotype approach to latest Cretaceous and earliest Tertiary paleosols in eastern Montana: *Geological Society of America Bulletin*, v. 106, p. 1377-1397, 10.1130/0016-7606(1994)106<1377:APATLC>2.3.CO;2.
- Retallack, G.J., 2001, *Soils of the past: an introduction to paleopedology*: Oxford; Malden, MA, Blackwell Science, 404 pp.
- Sheldon, N.D, and Retallack, G., 2002, Geochemical climofunctions from North American soils and application to paleosols across the Eocene-Oligocene boundary in Oregon: *Journal of Geology*, 110: 687-696, doi: 10.1086/342865.
- Soil Survey Staff, 1999, *Soil taxonomy: a basic system of soil classification for making and interpreting soil surveys*: U.S. Department of Agriculture-NRCS Agriculture Handbook 436, Second Edition: Washington, U.S. Government Printing Office, 869 p.
- Taylor, L.H., and Butler, R.F., 1980, Magnetic-polarity stratigraphy of Torrejonian sediments, Nacimiento Formation, San Juan Basin, New Mexico: *American Journal of Science*, v. 280, p. 97-115.
- Trendell, A.M., Atchley, S.C., and Nordt, L.E., 2012, Depositional and diagenetic controls on reservoir attributes within a fluvial outcrop analog: Upper Triassic Sonsela Member of the Chinle Formation, Petrified National Park, Arizona: *American Association of Petroleum Geologists, Bulletin*, v. 96, p. 679-707, doi: 10.1306/08101111025.
- Trendell, A.M., Atchley, S.C., and Nordt, L.C., 2013, Facies analysis of a probable large-alluvial-fan depositional fan: The Upper Triassic Chinle Formation at Petrified Forest National Park, Arizona, USA, v. 83, p. 873-895, doi: 10.2110/jsr.2013.55.
- Whittaker, R.H., 1975, *Communities and ecosystems*: New York, NY, USA, Macmillan, 385 pp.
- Wilf, P., 1997, When are leaves good thermometers? A new case for Leaf Margin Analysis. *Paleobiology* 23.3: 373-90.
- Wilf, P., Wing, S.L., Greenwood, D.R. and Greenwood, C.L., 1998, Using fossil leaves as paleoprecipitation indicators: an Eocene example: *Geology* 26: 203-206, doi: 10.1130/0091-7613(1998)026<0203:UFLAPI>2.3.CO;2.
- Williamson, T.E., 1996, The beginning of the age of mammals in the San Juan Basin, New Mexico: biostratigraphy and evolution of Paleocene mammals of the Nacimiento Formation: *New Mexico Museum of Natural History and Science Bulletin* 8:1-141.
- Williamson, T.E. and Lucas, S.G., 1992, Stratigraphy and mammalian biostratigraphy of the Paleocene Nacimiento Formation, southern San Juan Basin, New Mexico: *New Mexico Geological Society Guidebook* 43, p. 265-296.

- Williamson, T.E., Crossey, L.J., and Lucas, S.G., 1992, Silcretes of the Paleocene Nacimiento Formation, *in* S.G. Lucas, B.S. Kues, T.E. Williamson, and A.P. Hunt, eds., New Mexico Geological Society Guidebook, 43rd Field Conference, San Juan Basin IV, New Mexico Geological Society, p. 38-42.
- Williamson, T.E., Nichols, D.J., and Weil, A., 2008, Paleocene palynomorph assemblages from the Nacimiento Formation, San Juan Basin, New Mexico, and their biostratigraphic significance: *New Mexico Geology*, v. 30, p. 3-11.
- Wood, H.E., Chaney, R.W., Clark, J., Colbert, H., Jepsen, G.L., Reeside, J.B., and Stock, C., 1941, Nomenclature and correlation of the North American continental Tertiary, *Bulletin of the Geological Society of America*, v. 52, p. 1-48, doi: 10.1130/GSAB-52-1.
- Zachos, J., Pagani, M., Sloan, L., Thomas, E., and Billups, K., 2001, Trends, rhythms, and aberrations in global climate changes 65 Ma to present, *science*, v. 292, p 686-693, doi: 10.1126/science.1059412.